



# An organoid-based drug screening identified a menin-MLL inhibitor for endometrial cancer through regulating the HIF pathway

Jingyao Chen<sup>1</sup> · Lei Zhao<sup>1</sup> · Hongling Peng<sup>2</sup> · Siqi Dai<sup>1</sup> · Yuan Quan<sup>1</sup> · Manli Wang<sup>1</sup> · Jian Wang<sup>1</sup> · Zhanying Bi<sup>1</sup> · Ying Zheng<sup>2</sup> · Shengtao Zhou<sup>2</sup> · Yu Liu<sup>1</sup> · Chong Chen<sup>1</sup>  · Feifei Na<sup>1</sup>

Received: 27 January 2020 / Revised: 27 May 2020 / Accepted: 23 June 2020  
© The Author(s), under exclusive licence to Springer Nature America, Inc. 2020

## Abstract

Tumor organoids recapitulate pathological properties and would serve as an excellent *ex vivo* model for drug discovery. Here, we performed an unbiased drug screening on drivers-defined tumor organoids from mouse endometrial cancer, the most prevalent gynecological malignancy in human, with a small molecule library targeting epigenetic factors. Among them, menin-MLL inhibitors MI-136 and MI-463 scored. The therapeutic capacity of MI-136 was further validated in tumor organoids *in vitro* and an orthotopic model *in vivo*. CRISPR/cas9-mediated mutations of major components of the menin-MLL complex, *Men1*, *Kmt2a* and *Ash2l*, inhibited the growth of tumor organoids, suggesting that the complex was the target of MI-136. Transcriptome analysis showed that the hypoxia-inducible factor (HIF) pathway was the most significantly downregulated pathway by MI-136 treatment. Consistently, *Men1*, *Kmt2a*, and *Ash2l* knockout also repressed the expressions of the HIF target genes. Loss of *Hif1a* or *Hif1b* partially phenocopied the inhibition of the menin-MLL complex by MI-136 or mutations in term of tumor organoid growth. Further, we found that *MEN1* was upregulated in human endometrial cancers, which were tightly correlated with the expression levels of *HIF1A*, and associated with poor prognosis. Importantly, MI-136 also significantly inhibited the growth of endometrial cancer organoids derived from patients. Thus, our study identified MI-136 as a potential inhibitor for endometrial cancer through regulating the HIF pathway, a novel molecular mechanism distinguished from those in AML and prostate cancer.

## Background

Endometrial cancer is a lethal malignancy originating from the endometrial epithelial tissue [1]. It accounts for ~20–30% of female reproductive tract cancers and is one of the very few human cancers with increased incidences during last two decades [2]. The recurrence and

metastasis rates of stage III patients are high after treatment and the prognosis is extremely poor. The 5-year survival rate of stage III patients is ~40%, and that of stage IV patients is 5–15% [3]. There is an unmet need for effective treatment for endometrial cancer [4]. Though hormonal therapy has been a ‘standard’ treatment for these patients for four decades, endometrioid histology limits its therapeutic population [5]. Women with advanced endometrial cancer for whom treatment failed with first-line therapies have few treatment options [5].

Recent genomic studies have found a large number of genetic and epigenetic alterations in endometrial cancers [6, 7]. *TP53*, *PTEN*, *PIK3CA*, *FBXW7*, and *KRAS* are frequently mutated in human endometrial cancers [6, 8]. *PTEN* mutations often co-occurred with other mutations in the PI3K/AKT pathway [7, 9, 10]. Loss of *PTEN* function leads to upregulation of the PI3K/AKT/mTOR pathway, which promotes cell growth [11]. *TP53* mutations or loss happen in almost all type II endometrial cancer patients and are strongly associated with poor

**Supplementary information** The online version of this article (<https://doi.org/10.1038/s41417-020-0190-y>) contains supplementary material, which is available to authorized users.

- ✉ Chong Chen  
chongchen@scu.edu.cn
- ✉ Feifei Na  
nafeifei@foxmail.com

<sup>1</sup> Department of Thoracic Oncology, State Key Laboratory of Biotherapy and Cancer Center, West China Hospital, Sichuan University, Chengdu, China

<sup>2</sup> West China Second Hospital, Sichuan University, Chengdu, China

prognosis [3]. *TP53* mutations often accompany extensive copy number alterations, low ER/PR levels and few DNA methylation changes in uterine serous tumors and ~25% of high-grade endometrioid cancer [7].

Besides genetic mutations, epigenetic alterations, including both histone modifications and DNA methylations, are also underlying the pathology of human endometrial cancers [12]. Promoter hypermethylation is associated with downregulated expressions of target genes, such as tumor suppressors *PTEN* [13], *RSK4* [14], *APC* [15, 16], and *CDKN2A* [17, 18]. In addition, changes in CpG island and expressions of DNMTs have been found in endometrial cancer, all of which can lead to DNA methylation changes [19, 20]. Histone modification enzymes, including histone deacetylases (HDACs), histone acetyltransferases (HATs), histone methyltransferases (HMTs), and histone demethylases (HDMs), are frequently dysregulated in endometrial cancer and associated with tumor aggressiveness features [21–25]. Though the potential functions and detailed mechanisms of these epigenetic abnormalities have not been fully understood, these epigenetic abnormalities may give rise to susceptibilities for endometrial cancer, which can be new targets for treatments.

Previous studies on endometrial cancer largely relied on 2-D cultured cell lines [26]. Tumor cell lines are insufficient to represent the clinic pathologies of this disease. Recently, tumor organoids have been developed as 3D cultured *ex vivo* structures from biopsies of patients or model animals [27]. It has been shown that tumor organoids can precisely recapitulate most of the characteristics of the disease, including genetic mutations, cellular components and, most importantly, responses to clinic drug treatments [28–30]. Both normal and tumor organoids have also been successfully developed from human and mouse endometrial tissues [31, 32]. Patient-derived endometrial cancer organoids accurately replicate the genetic mutational landscape and represent patient-specific drug responses. However, given the heterogeneity among individuals, it is challenging to generalize the studies from patient-derived organoids. In this case, tumor organoids driven by defined genetic drivers from model animals were of value to identify therapeutic targets and inhibitors for a group or subgroup of diseases.

In the present study, we generated an orthotopic primary endometrial cancer mouse model driven by *Trp53*, *Pten*, and *Pik3r1* loss and developed drivers-defined tumor organoids from this model. An epigenetic drug library screening was performed on these organoids. One of the top candidates from the screening was further validated *in vitro* and *in vivo* and the potential underlying molecular mechanism was explored by transcriptional and epigenetic analysis.

## Results

### Organoid-based small molecule screening with an epigenetic drug library for endometrial cancer

Tumor organoids have been shown being able to better represent the characteristics of the diseases than other *in vitro* models and therefore be of value for identifying potential drugs for human cancers [29, 32]. However, the heterogeneity among patients dramatically increases the complexity of drug screening with tumor organoids. To simplify tumor organoid-based drug library screening, we decided to develop drivers-defined endometrial cancer organoids from orthotopic primary mouse endometrial cancer model and then perform small molecule library screening on these tumor organoids (Fig. 1a). Firstly, we generated a drivers-defined mouse endometrial cancer model with mutations on *Trp53*, *Pten* and *Pik3r1* and overexpressions of *Myc* and *Kras*<sup>G12D</sup> (published elsewhere), which could represent the majority of human endometrial cancers with poor prognosis. Cancer cells from freshly dissected mouse endometrial cancer self-organized into a 3D structure in culture medium with matrigel (Fig. 1b). These endometrial cancer organoids could be maintained and passaged stably infinitely. Hematoxylin & Eosin staining showed histology of the tumor organoids, including atypical nucleus, resembling that of high grade endometrial cancer in patients (Fig. 1b).

A small molecule library of 276 compounds, targeting epigenetic factors including histone methyltransferases, demethylases, DNA methyltransferases and epigenetic readers, was used (Fig. 1c). Endometrial cancer organoids were cultured in 96-well plates. Each inhibitor was added into two replicate wells at the concentration of 10  $\mu$ M. Three days later, the surviving organoids were quantified by Cell counting kit-8 (CCK-8), a sensitive mitochondrial activity-based assay for cell viability. Inhibition scores for each drug were determined by comparing to that of vehicle-treated organoids (Fig. 1d). 11 drugs completely abolished the growth of tumor organoids, 25 reduced the organoid growth to <10% of control, and 41 reduced to 10–50% (Fig. 1e). The compounds that induced >50% inhibition in the endometrial cancer organoids were enriched in those targeting HDAC, Aurora Kinase and DNA/RNA synthesis, consistent with previous reports and thus validating our screening [33–35]. It is interesting that the top categories that completely inhibited the growth of tumor organoids were those targeting HMTs. Among the three HMT inhibitors, MI-136 caught our attention because it has recently been shown to be able to treat prostate cancer and leukemia and several drugs targeting the same target, the menin-MLL complex, are tested in clinical trials (Fig. 1f, g) [36–38]. Thus, we decided to further investigate this inhibitor in endometrial cancer.

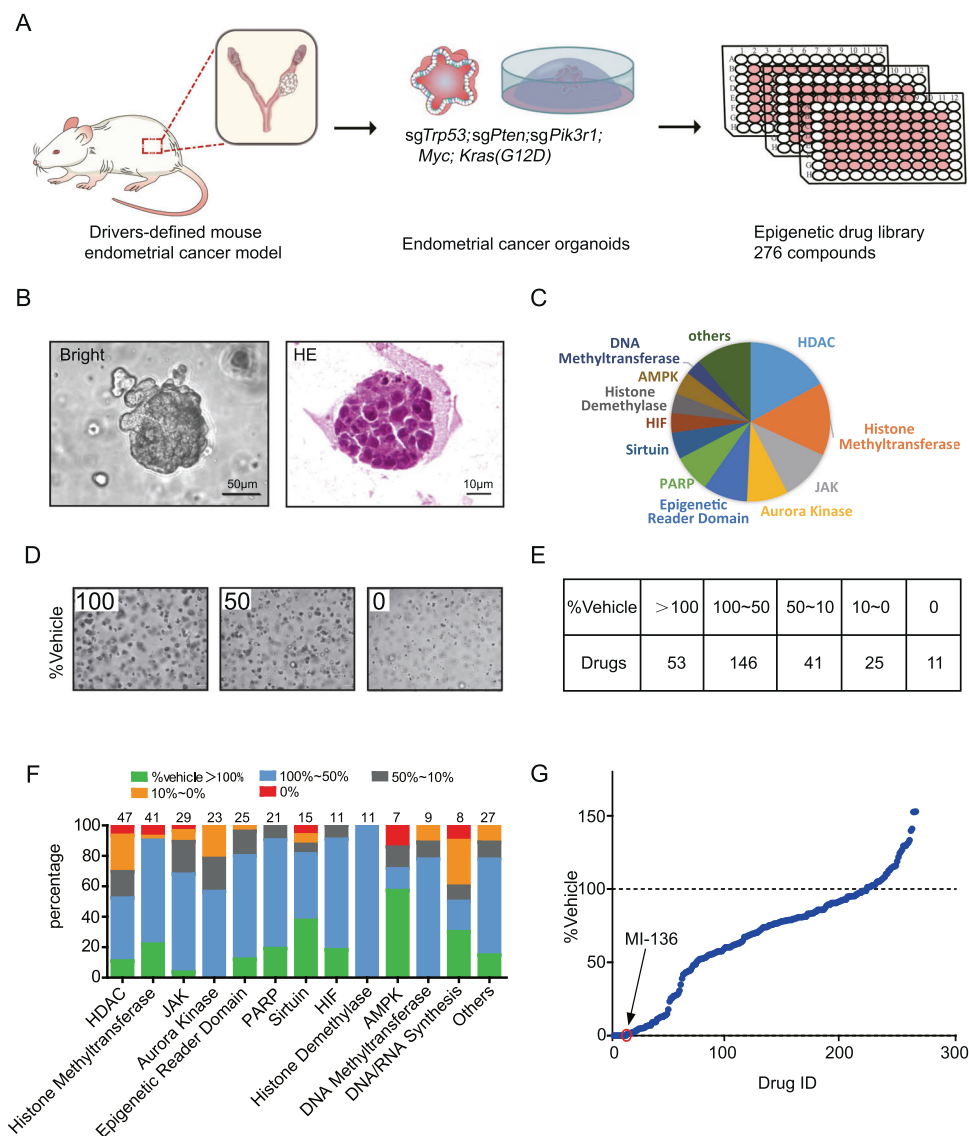


**Fig. 1 Organoid-based small molecule screening with an epigenetic drug library for endometrial cancer.** **a** Schematic of the high-throughput epigenetic drug Screening. Endometrial cancer cells derived from a primary orthotopic mouse model were cultured with matrigel in 96-well plates. After 24 h of culture, organoids were treated with compounds from an epigenetic drug library of 276 compounds individually. After 72 h of treatment, imaging assay was used to determine organoid number and size. And then, cell viability was analyzed by CCK8 assay. **b** Left, bright-field image of endometrial cancer organoids, showing morphological characteristics. Scale bar, 50 µm. Right, Haematoxylin and Eosin (H&E) staining of endometrial

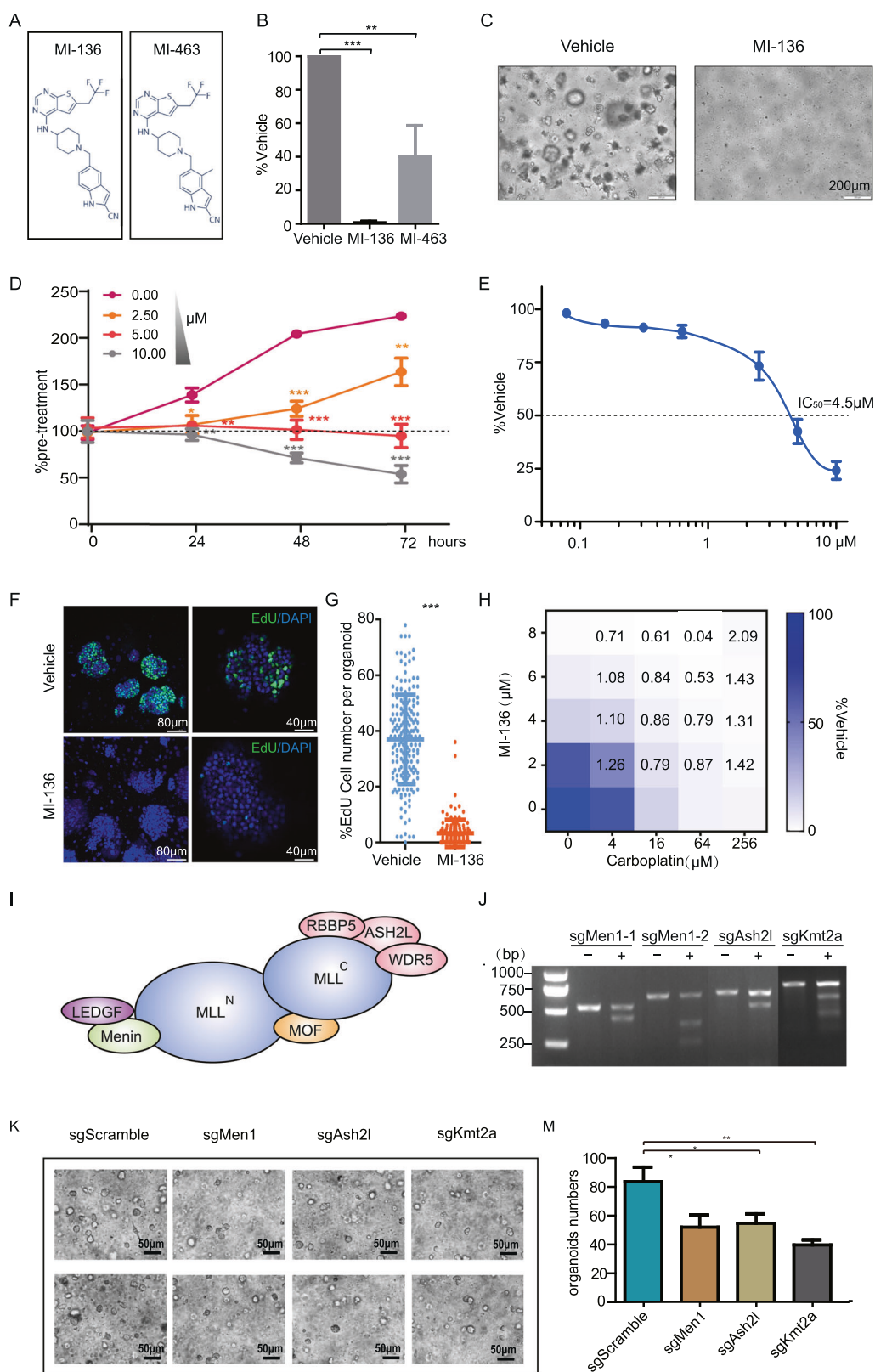
cancer organoids. Scale bar, 10 µm. **c** Summary of drug classification in the epigenetic drug library. **d** Representative images of tumor organoids with the proportions of cell viability at 0%, 50%, and 100%, relative to that of the vehicle treated ones. **e** The numbers of drugs with which the survival ratios were 0%, 0–10%, 10–50%, 50–100% and more than 100%, relative to the vehicle group. **f** Incidence of cell viability at 0%, 0–10%, 10–50%, 50–100% and more than 100% after treatment in each kind of target. The numbers above the bars indicated the drug numbers in this class. **g** Summary of the drug library screening showing the relative survival ratios of tumor organoids treated with individual drug.

### Menin-MLL inhibitor MI-136 inhibited the growth of endometrial cancer organoids

Interestingly, two independent menin-MLL inhibitors, MI-136 and MI-463, were among the top candidates (Fig. 2a). MI-136 had nearly 100% inhibitory effect for endometrial cancer organoid growth, while MI-463 ~50% inhibition ratio (Fig. 2b, c). Menin-MLL inhibitors have been shown to be

effective for MLL-rearranged leukemia [36, 37] and androgen receptor-dependent prostate cancer [38]. We wonder if these inhibitors would hold promise for endometrial cancer, a female malignancy driven by distinct mechanism.

Firstly, we performed a validation experiment and confirmed the strong inhibition of MI-136 on endometrial cancer organoid growth (Fig. 2d). Then, we titrated the concentrations of MI-136 and found that as low as 2.5 µM



MI-136 could significantly reduce the growth of endometrial cancer organoids. Higher concentrations of MI-136 (5 and 10  $\mu$ M) completely inhibited the growth and

further induced the death of tumor organoids (Fig. 2d). IC<sub>50</sub> of MI-136 on these endometrial cancer organoids was 4.5  $\mu$ M (Fig. 2e).

◀ **Fig. 2 Menin-MLL inhibitor MI-136 inhibited the growth of endometrial cancer organoids in vitro.** **a** Chemical structures of the Menin-MLL inhibitors MI-136 and MI-463. **b** The proportions of cell viability treated with MI-136 or MI-463 at 10  $\mu$ M, relative to that of vehicle treated organoids.  $n = 3$ . Error bars represent SD.  $**p < 0.01$ ;  $***p < 0.001$ . **c** Representative images of endometrial cancer organoids treated with vehicle or MI-136 at 10  $\mu$ M. Scale bars, 200  $\mu$ m. **d** The growth curves showing numbers of tumor organoids treated with MI-136 of indicated concentrations over time.  $n = 3$ . Error bars represent SD.  $*p < 0.05$ ;  $**p < 0.01$ ;  $***p < 0.001$ . **e** Drug dose response curve showing cell viability of endometrial cancer organoids in response to 72 h treatment of MI-136.  $IC_{50}$  was shown.  $n = 3$ . Error bars represent SD.  $***p < 0.001$ . **f** Representative images of EdU staining of endometrial cancer organoids treated with vehicle or MI-136 for 18 h. Scale bar, 80 and 40  $\mu$ m. **g** Densitometric analysis of EdU levels normalized to DAPI levels in endometrial cancer organoids, calculated with Imaris software. Error bars represent SD.  $***p < 0.001$ . **h** Relative survival of endometrial cancer organoids treated with combinations of MI-136 and Carboplatin at indicated concentrations. The numbers in the color block indicated the combination index. **i** Schematic of the structure of the menin-MLL complex. **j** T7E1 endonuclease 1 (T7E1) assays on *Men1*, *Ash2l*, and *Kmt2a* using infected cancer organoid. **k** Representative images of mouse endometrial cancer organoids expressing sgScramble, sg*Men1*, sg*Ash2l* or sg*Kmt2a*, measured at 48 h after infection. Scale bar, 50  $\mu$ m. **m** The organoid numbers expressing sgScramble, sg*Men1*, sg*Ash2l* or sg*Kmt2a*.  $n = 3$ . Error bars represent SD.  $*p < 0.05$ ;  $**p < 0.01$ ;  $***p < 0.001$ .

To measure the effect of MI-136 on the proliferation of tumor organoids, we performed EdU incorporation assay. Half of the tumor cells in untreated organoids were EdU positive, indicating high proliferating feature of our endometrial cancer cells. In striking contrast, after 18 h of treatment with 10  $\mu$ M MI-136, EdU incorporation was completely abolished, suggesting that MI-136 prevented endometrial cancer growth mainly through inhibiting proliferation (Fig. 2f, g).

Further, we tested the potential combination effect of MI-136 with carboplatin, a first-line chemotherapy drug for endometrial cancer. When applied with carboplatin, MI-136 could significantly inhibit the growth of endometrial cancer organoids at much lower concentrations, suggesting a potential combination therapy of MI-136 (Fig. 2h).

To confirm the menin-MLL complex as bona fide therapeutic target in endometrial cancer, we tested whether deficiencies of the major components of this complex, *Men1*, *Kmt2a* and *Ash2l*, by CRISPR/Cas9 would impair the growth of tumor organoids (Fig. 2i). We introduced Cas9 and sgRNAs targeting *Men1*, *Kmt2a* or *Ash2l* into tumor organoids with lentivirus. T7E1 assay showed that *Men1*, *Kmt2a* and *Ash2l* were efficiently disrupted by CRISPR/cas9 (Fig. 2j). Consistently with MI-136 treatment, mutations of *Men1*, *Kmt2a* and *Ash2l* significantly inhibited tumor organoid growth, compared to organoids with sgRNA-scramble (Fig. 2k–m). Thus, MI-136 is a potent inhibitor for endometrial cancer by targeting the menin-MLL complex.

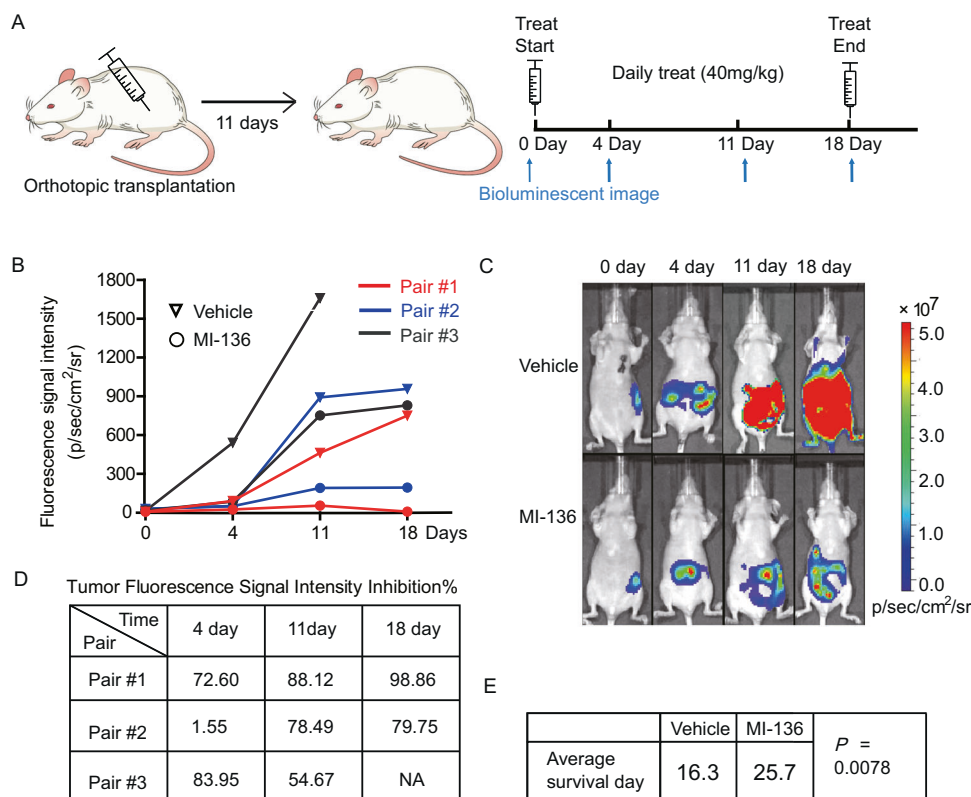
## MI-136 inhibited Tumor Growth in an orthotopic endometrial cancer mouse model

To test the effect of MI-136 in vivo, we generated an orthotopic endometrial cancer mouse model by injecting the above endometrial cancer organoids into the uterus of 8-week-old nude mice. These cancer organoids were luciferase-expressing and therefore we could monitor the growth of these orthotopic tumors by bioluminescence imaging. MI-136 was delivered by daily intraperitoneal injections at 40 mg/kg bodyweight, following a protocol for prostate cancer as reported [38]. Bioluminescence imaging was taken once per week (Fig. 3a). To reduce the effect of the variations of tumor sizes before treatment, we paired the animals by the initial fluorescence signal intensity. A total of 3 pairs of recipient mice were treated with MI-136 or vehicle. In Pair#1, the initial fluorescence signal intensity was  $7.28 \times 10^5$  (Vehicle) and  $6.41 \times 10^5$  (MI-136), respectively. The tumor in the vehicle-treated mouse grew rapidly, indicated by dramatically increased fluorescence signal intensity to  $9.15 \times 10^6$  at 4 days,  $4.63 \times 10^7$  at 11 days and  $7.51 \times 10^7$  at 18 days (Fig. 3b). In contrast, the MI-136 treated tumor barely grew during the period of 18-day treatment and was inhibited by 72.60% at 4 days, 88.12% at 11 days and 98.86% at 18 days (Fig. 3d). Similar inhibition of tumor growth was also observed in Pair#2 and Pair#3 (Fig. 3b, c). The average inhibition ratios of tumor growth by MI-136 were 52.70% at 4 days, 73.76% at 11 days and 89.31% at 18 days (Fig. 3d). The treatment stopped at day 18 for some control animals died or were too weak. The average survival of MI-136 treated mice were 26 days, comparing to 16 days of vehicle treated ones ( $p = 0.0078$ ) (Fig. 3e). Taken together, these results demonstrated that menin-MLL inhibitor MI-136 substantially delayed progression of endometrial cancer in vivo.

## MI-136 treatment inhibited the HIF signaling pathway

In MLL-rearranged AML, MI-136 directly breaks the interaction of menin with MLL-fusion proteins and thus represses the expressions of MLL-fusion downstream *HOX* genes [37]. In prostate cancer, MI-136 inhibits tumor growth by repressing menin-MLL complex mediated androgen signaling [38]. Since there are neither MLL-fusion protein nor androgen signaling functions in endometrial cancer, MI-136 must work through a different mechanism in this gynecological malignancy. To explore the molecular mechanism of MI-136 on endometrial cancer, we performed RNA-sequencing analysis to compare the transcriptomes of endometrial cancer organoids treated with MI-136 or vehicle. There were 580 and 777 genes significantly up- and down-regulated, respectively, in

**Fig. 3 MI-136 repressed in vivo tumor growth in an orthotopic endometrial cancer model.** **a** Schematic of experimental workflow to evaluate the effect of MI-136 on tumor growth in mice with orthotopic endometrial cancers. **b** Luciferase fluorescence signal intensity Pair#1-3 recipient mice before and after MI-136 or vehicle treatments by bioluminescence imaging. **c** Representative luciferase fluorescence images of recipient mice (Pair#1) before and after MI-136 or vehicle treatments by bioluminescence imaging. **d** The percentages of in vivo growth inhibition of tumor treated with MI-136, compared to that of paired tumor treated with vehicle, measured by luciferase fluorescence signal intensity. **e** Average survival (days) of mice with endometrial cancers treated with vehicle or MI-136.



endometrial cancer organoids after 12 h of treatment with 10  $\mu$ M MI-136 (Fig. 4a).

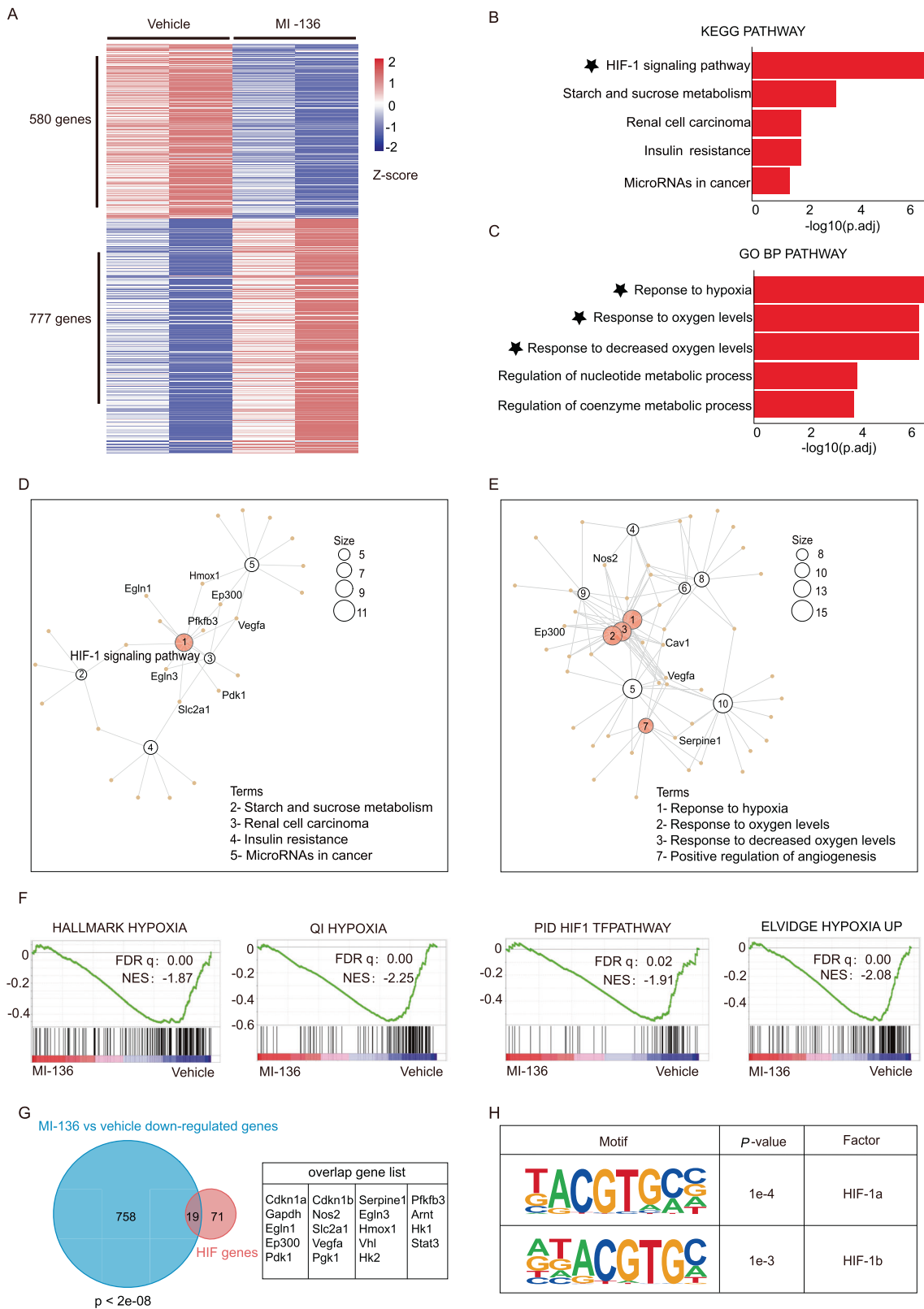
Interestingly, KEGG pathway analysis revealed that the HIF-1 signaling pathway was the top one enriched in downregulated genes ( $p_{\text{adj}} = 4.9\text{e-}07$ ) (Fig. 4b). Consistently, GO Analysis also showed that multiple HIF-related pathways, including response to hypoxia, response to oxygen levels and response to decreased oxygen levels, were significantly enriched in downregulated genes, aside with proliferation-related pathways (Fig. 4c). Regulatory network analysis of these enriched KEGG pathways and GO BP pathways with ClusterProfiler further demonstrated that the HIF pathway was the most significantly enriched pathway downregulated by MI-136 (Fig. 4d, e). Gene set enrichment analysis (GSEA) indicated that all of the Hallmark Hypoxia gene set (NES = -1.87, FDR  $q = 0.00$ ), QI\_Hypoxia gene set (NES = -2.25, FDR  $q = 0.00$ ), PID\_HIF1\_TF gene set (NES = -1.91, FDR  $q = 0.02$ ) and Elvidge\_Hypoxia\_up gene set (NES = -2.08, FDR  $q = 0.00$ ) were significantly negatively enriched in endometrial cancer organoids treated with MI-136, compared to those with vehicle (Fig. 4f).

Indeed, 19 out of the 90 bona fide HIF target genes, including *Arnt*, *Egln1*, *Egln3*, *Hkl* and *Hk2*, were downregulated for more than 1.3-fold by MI-136 ( $p < 2\text{e-}08$ ) (Fig. 4g). Motif discovery analysis by HOMER showed that both HIF-1a and HIF-1b binding motives

were significantly enriched in MI-136 downregulated genes ( $p = 1\text{e-}4$  and  $1\text{e-}3$ , respectively) (Fig. 4h). Overall, these results demonstrated that menin-MLL inhibitor MI-136 inhibited HIF signaling pathway in mouse endometrial cancer organoids.

### Menin directly bound at HIF target genes and regulated their expressions

The menin-MLL complex can directly bind on the promoters and coding regions of its target genes. We wondered if these HIF pathway genes downregulated by MI-136 would be direct targets of the menin-MLL complex. We analyzed ChIP-seq data with antibodies against menin in prostate cancer cells (accession codes: GSM3893168, GSM3893171) and breast cancer cells (GSM2264617, GSM2264618, GSM2264619, GSM2264620). We found that most of these MI-136 downregulated genes had significant binding of menin on their promoters and coding regions (Fig. 5a–d) (Supplemental Fig. 1). Specifically, nitric oxide synthase 2 and 3 (*Nos2/3*) are directly transcriptionally regulated by HIF and can promote the proliferation and tumorigenic angiogenesis of multiple cancer cells [39, 40]. Menin bound on both the promoters and coding regions of *Nos2* and *Nos3* (Fig. 5a, b). Consistently, the expressions of both *Nos2* and *Nos3* were significantly reduced in MI-136 treated endometrial cancer organoids,



measured by both RNA-seq and qRT-PCR (Fig. 5a, b). The glycolytic enzyme 6-phosphofructo-2-kinase/fructose-2,6-biphosphatase 3 (*Pfkfb3*), a transcriptional target of HIF, is

upregulated in several cancers and proposed to be potential therapeutic target for cancer treatment [41, 42]. Menin also could directly bind on its promoter and coding region and

◀ **Fig. 4 MI-136 treatment inhibited the HIF signaling pathway in endometrial cancer organoids.** **a** Heatmap showing the differentially expressed genes between mouse endometrial cancer organoids treated with vehicle or MI-136 for 12 h, measured by RNA-seq. **b** Bar plots showing the most enriched KEGG pathways in the downregulated genes in endometrial cancer organoids treated with MI-136, comparing to those with vehicle. **c** Bar plots showing the most enriched GO pathways in the downregulated genes in endometrial cancer organoids treated with MI-136, comparing to those with vehicle. \* indicating the HIF-related pathways. **d** Regulatory Network of enriched KEGG pathways, analyzed with ClusterProfiler. Circle sizes for enriched pathways represent the numbers of genes enriched in these pathways. **e** Network analysis of enriched GO BP pathways, analyzed with ClusterProfiler. Circle sizes for enriched pathways represent the numbers of genes enriched in these pathways. **f** Gene set enrichment analysis (GSEA) of Hallmark hypoxia, Qi hypoxia, PID HIF1 TF pathway and Elvidge hypoxia up in endometrial cancer organoids treated with MI-136, comparing to those with vehicle. **g** Left, Venn diagram showing the overlapping of downregulated genes in MI-136 treated organoids with the HIF signaling pathway genes. Right, the gene symbols of overlapped genes. **h** The enriched binding site sequences of downregulated genes by MI-136, analyzed by HOMER.

MI-136 treatment significantly reduced the expression of *Pfkfb3* in endometrial cancer organoids (Fig. 5c). Similarly, Caveolin-1 (*Cav1*), an oncogenic protein [43] transcriptionally regulated by HIF1a, was also bound by menin and downregulated by MI-136 (Fig. 5d).

Importantly, we showed that, the expressions of these HIF target genes, *Nos2*, *Nos3*, *Cav1*, and others, which were repressed in tumor organoids by MI-136 treatment and regulated by menin, were also significantly reduced in organoids with *Men1*, *Kmt2a* or *Ash2l* loss (Fig. 5e). These data suggested that multiple HIF pathway genes were directly regulated by the menin-MLL complex and inhibition of the menin-MLL interaction by MI-136 transcriptionally downregulated the HIF pathway.

Further, to test the potential roles of the HIF pathway as mediators of the menin-MLL complex in endometrial cancer, we knocked out *Hif1a* and *Hif1b* in tumor organoids with CRISPR/cas9. We found that loss of either *Hif1a* or *Hif1b* significantly inhibited the growth of tumor organoids, compared with those with sgRNA-scramble (Fig. 5f). Consistently, *Hif1a* and *Hif1b* deficiencies also had similar effects on the expressions of MI-136 regulated genes, *Nos2*, *Nos3*, *Cav1*, *Sperpines1* and many others (Fig. 5g). Thus, targeting the menin-MLL complex impaired the growth of endometrial cancer through inhibiting the HIF pathway.

### The menin-HIF axis was upregulated in human endometrial cancer and MI-136 inhibited the growth of human endometrial cancer organoids

Then we wondered whether the molecular mechanism and treatment strategy that we found in mouse endometrial

cancer would be upheld in human patients. We analyzed the transcriptomic data of human endometrial cancer, comparing to normal endometrial tissues, in TCGA cohort. Both *MEN1* and *HIF1A* were significantly upregulated in human endometrial cancer than normal tissues ( $p < 2.2e-16$  and  $p = 0.00028$ , respectively) (Fig. 6a). Strikingly, there was a strong positive correlation between the expression levels of *MEN1* and *HIF1A* in patients ( $R = 0.4$ ,  $p < 2e-16$ ) (Fig. 6b). More importantly, high level of *MEN1* was significantly associated with poor prognosis in terms of both overall survival and relapse-free survival in endometrial cancer patients (Fig. 6c, d). These data suggested that the MEN1-HIF axis was activated in human endometrial cancer and predicted a poor outcome.

Then, we tested the therapeutic effect of MI-136 in human endometrial cancer. We successfully cultured tumor organoids from four endometrial cancer patients and treated them with or without MI-136. The growth of these organoids was measured by both CCK-8 for cell viability and the numbers of surviving tumor organoids were counted. In all cases, MI-136 strongly reduced cell viability and organoid numbers of human endometrial cancer organoids for at least 60% (Fig. 6e–h). Thus, the menin-MLL inhibitor MI-136 was effective to inhibit the growth of not only mouse endometrial cancer but also human endometrial cancer.

## Discussion

In this study, we constructed a new drug discovery pipeline for endometrial cancer through small molecule library screening based on drivers-defined tumor organoids. As an example, we performed a screening with 276 epigenetic inhibitors. Though epigenetic abnormalities are frequent in human endometrial cancer, there are few epigenetic therapeutic targets or inhibitors identified for this notorious disease [12, 25]. Besides many other known inhibitors, our screening identified an unexpected inhibitor MI-136. MI-136 is a specific inhibitor for the menin-MLL complex. It has been shown to be potent on MLL-fusion driven AML and prostate cancer [36, 38]. But this inhibitor and its target the menin-MLL complex have not been studied in endometrial cancer. We showed that MI-136 strongly inhibited endometrial cancer both ex vivo and in vivo, and also human tumor organoids. Several menin-MLL inhibitors, including KO-539 and SNDX-5613, are in clinical trials for leukemia patients. Further testing these inhibitors in future clinical trials on endometrial cancer would provide new promise for patients.

Previous studies on menin-MLL complex and its inhibitors were focused on MLL-arranged AML [37, 44] and androgen receptor-dependent prostate cancer [38]. In AML with MLL translocations, menin directly binds with MLL

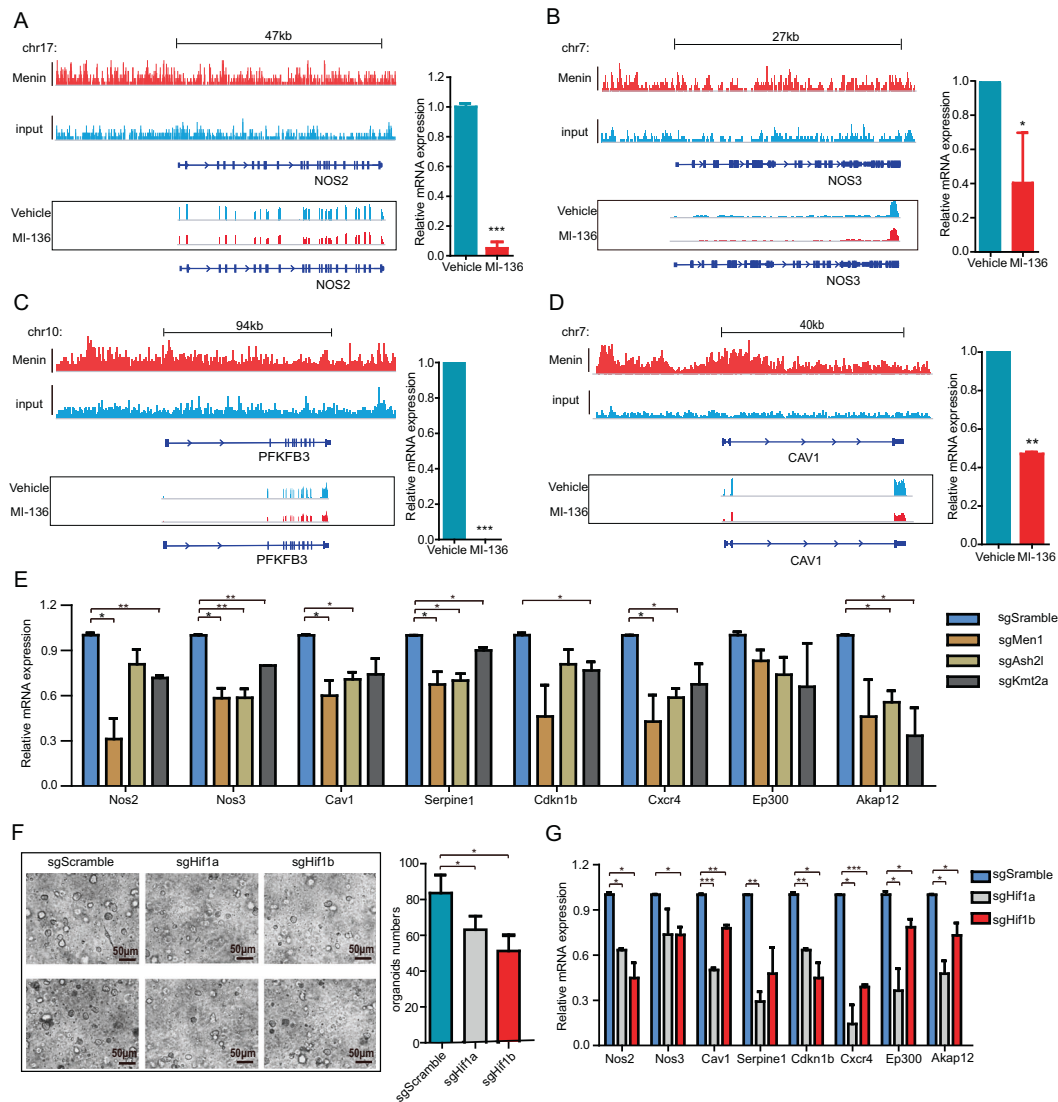


**Fig. 5** Menin directly bound on the promoters and gene bodies of multiple HIF pathway genes which were downregulated by MI-136. **a–d** Left, the binding peaks of menin on *NOS2* (**a**), *NOS3* (**b**), *PFKFB3* (**c**) and *CAV1* (**d**), measured by ChIP-seq (GSE132827) and the RNA-seq reads in endometrial cancer organoids treated with vehicle or MI-136. Right, the relative expression level of *Nos2* (**a**), *Nos3* (**b**), *Pfkfb3* (**c**) and *Cav1* (**d**), in MI-136 treated endometrial cancer organoids, comparing to that of vehicle, measured by qRT-PCR.  $n = 3$ . Error bars represent SD. \* $p < 0.05$ ; \*\* $p < 0.01$ ; \*\*\* $p < 0.001$ . **e** The relative expression level of *Nos2*, *Nos3*, *Cav1*, *Serpine1*, *Cdkn1b*, *Cxcr4*, *Ep300* and *Akap12* in endometrial cancer organoids expressing sgMen1, sgAsh2l, sgKmt2a, comparing to organoids

expressing sgScramble, measured by qRT-PCR.  $n = 3$ . Error bars represent SD. \* $p < 0.05$ ; \*\* $p < 0.01$ ; \*\*\* $p < 0.001$ . **f** (Left) Representative images of mouse endometrial cancer organoids expressing sgScramble, sgHif1a or sgHif1b, measured at 48 h after infection. Scale bar, 50 μm. (Right) The organoid numbers expressing sgScramble, sgHif1a or sgHif1b.  $n = 3$ . Error bars represent SD. \* $p < 0.05$ ; \*\* $p < 0.01$ ; \*\*\* $p < 0.001$ . **j** The relative expression level of *Nos2*, *Nos3*, *Cav1*, *Serpine1*, *Cdkn1b*, *Cxcr4*, *Ep300* and *Akap12* in endometrial cancer organoids expressing sgHif1a or sgHif1b, comparing to organoids expressing sgScramble, measured by qRT-PCR.  $n = 3$ . Error bars represent SD. \* $p < 0.05$ ; \*\* $p < 0.01$ ; \*\*\* $p < 0.001$ .

fusion proteins and upregulates the expressions of *HOX* genes and thus its inhibitors disrupt the interaction between menin and MLL fusion protein and downregulated *HOX* genes. In prostate cancer, menin-MLL complex directly interacts with androgen receptor to drive a castration resistance program and menin-MLL inhibitors break the interaction and inhibit tumor growth. In our study, endometrial cancers, without either MLL fusion or androgen

receptor, also have high levels of *MEN1* expressions. More importantly, this disease depends on the activity of the menin-MLL complex, revealed by MI-136 treatment and mutations of the menin-MLL complex components, *Men1*, *Kmt2a*, and *Ash2l*, by CRISPR/cas9. By transcriptome and epigenetic analyses, we showed that the menin-MLL complex directly regulated the expressions of multiple components of the HIF pathway. Pharmaceutical and genetic

### Fig. 6 Analysis of the menin-HIF axis in human

#### endometrial cancers and the effect of MI-136 on the growth of patient-derived endometrial cancer organoids.

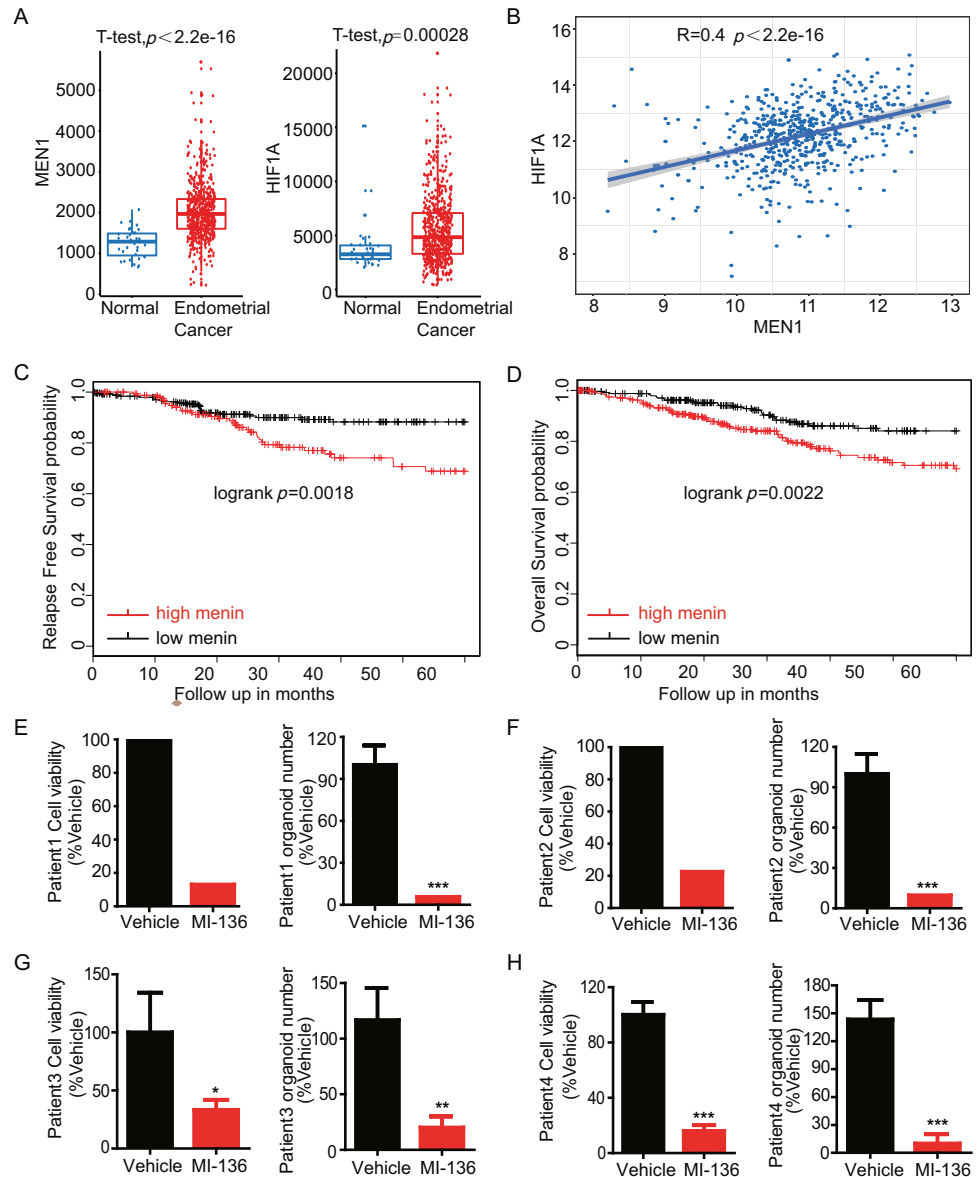
**a** The expression levels of *MEN1* and *HIF1A* in human normal endometrium ( $n = 35$ ) and endometrial cancers ( $n = 587$ ), analyzed from The Cancer Genome Atlas. **b** The correlation of *MEN1* and *HIF1A*

expressions in human endometrial cancers. **c**

Kaplan–Meier relapse free survival curve of endometrial cancer patients with low or high expressions of *MEN1*. Patients were split by median on the basis of *MEN1* mRNA

expression. **d** Kaplan–Meier overall survival curve of endometrial cancer patients with low or high expressions of *MEN1*. Patients were split by median on the basis of *MEN1*

mRNA expression. **e–h** Relative cell viability and organoid numbers of Patient 1–4 tumor organoids treated with MI-136, comparing to those of vehicle. Error bars represent SD. \* $p < 0.05$ ; \*\* $p < 0.01$ ; \*\*\* $p < 0.001$ .



inhibitions of the menin-MLL complex downregulated the HIF pathway. Disruption of *Hif1a* or *Hif1b* mimicked the effects of MI-136 treatment. Thus, the HIF pathway is a key mediator of the menin-MLL complex in endometrial cancer. Taken together, our study revealed a novel molecular mechanism of the menin-MLL complex in endometrial cancer. It would be interesting to test whether the menin-MLL complex would directly bind with HIF1 and regulate their downstream targets in endometrial cancer cells.

## Conclusion

In summary, our study suggested a new treatment strategy and revealed the menin-HIF axis as an unexpected molecular mechanism for endometrial cancer. It would be

interesting to test whether the menin-HIF axis would also underlie the molecular mechanisms of other cancers.

## Material and methods

### Mouse organoid culture

The mouse uterus was removed, cut and digested with collagenase. After filtered through 100  $\mu\text{m}$  filter and collected by centrifugation, the fresh uterus cells were resuspended in ice-cold Matrigel (BD, 354230). The basal culture medium for mouse organoids was slightly modified from previously report [31]. Organoids were passaged every 3–5 days. Lentiviral plasmid encoding sgRNA targeting *Trp53*, *Pten* and *Pik3r1* were constructed. Retroviral

plasmid encoding cDNA of *Myc* and *Kras<sup>G12D</sup>* were constructed. Viral particles were generated. Organoids were infected with lentiviruses and retroviruses. After passage and genotype identification, infected organoids were injected into the left uterus of 8-week-old nude mice. Mice were monitored by bioluminescence imaging.

The mouse endometrial tumor was removed, minced into small pieces and placed into gentleMACS tube with 1.0 mg/ml Collagenase I/0.5 mg/ml Collagenase IV/DMEM/F12. Then the tube was put into a gentleMACS tissue processor and the Program *m\_lung\_01.02* was run. After that, detach the tube from the gentleMACS tissue processor, incubate sample with gentle shaking at 37 °C for 20–30 min, and then run the gentleMACS Program *m\_lung\_02.01*. The supernatant was passed through a 100- $\mu$ m cell filter (Corning, 431752) and the filter was washed several times with medium. The cells were collected by centrifugation, resuspended in ice-cold Matrigel (BD, 354230) at a ratio of 1:20 (vol:vol). Thirty-microlitre drops of Matrigel-cell suspension were plated into 48-well plates (Costar, 3548), overlaid with 150  $\mu$ l organoid Expansion Medium (ExM) and set at 37 °C. The ExM was changed every three days and they were passaged by manual pipetting every 5–7 days. The ExM was as follows: Advanced Dulbecco's modified Eagle medium/F12 was supplemented with penicillin/streptomycin, 2 mM Glutamax, 1  $\times$  B27 (Life Technologies), 1  $\times$  N2 (Life Technologies), 10 nM gastrin I (Sigma), 1 mM N-acetylcysteine (Sigma) and 10 mM Nicotinamide (Sigma). The following growth factors were used: 50 ng/ml mouse recombinant EGF, 100 ng/ml mouse recombinant noggin (Peprotech), 100 ng/ml mouse recombinant FGF10 (Peprotech), 125 ng/ml R-spondin-1 conditioned medium (Peprotech), 10% Wnt-3A conditioned medium, 500 nM A83-01 (Tocris).

### Human organoid culture and treatment

Patient-derived organoids from endometrial cancer were cultured as previously reported [32]. The study was approved by the Ethical Research Committee of the West China Second Hospital (2017SZ0064).

Cells were seeded into 96-well plates at 3000 per well. In all, 24 h later, MI-136 were added into three replicate wells at the concentration of 10  $\mu$ M. Three days after treatment, we took four bright-field images for each well. The numbers of surviving tumor organoids per image were counted. After that, the survived organoids were quantified by Cell counting kit-8 (CCK-8), a sensitive mitochondrial activity-based assay for cell viability. Inhibition scores were determined by comparing to vehicle-treated wells.

### Drug screening

Drivers-defined mouse endometrial cancer organoids were subjected to a drug screen with Epigenetics Compound Library (Selleckchem, 276 compounds in total). Tumor organoids were recovered from Matrigel and dissociated in TrypLE. Cells were seeded into 96-well plates at 3000 per well. In all, 24 h later, inhibitors were added into two replicate wells at the concentration of 10  $\mu$ M. Three days after treatment, the survived organoids were quantified by Cell counting kit-8 (CCK-8). Inhibition scores for each drug were determined by comparing to vehicle-treated wells.

In the primary screen, 276 drugs are ranked according to the inhibition score. Drugs with inhibition score <20% were selected as the candidates. In the second screen, cells were seeded into 96-well plates at 3000 per well. In all, 24 h later, the candidates were added into two replicate wells at the concentration of 1  $\mu$ M. Three days after treatment, a few drugs were identified according to the inhibition score. For validation, they were added at various concentrations and viability was measured after 72 h. The vehicle (DMSO; D8418, Sigma Aldrich) was used as a negative control.

### Combination index

The combination index of MI-136 and carboplatin was calculated according to the described protocol [45].

### Mice and in vivo treatment

All the mouse experiments were approved by the institutional Animal Care and Use Committees of Sichuan University. For in vivo treatment studies,  $\sim 2 \times 10^6$  *sgTrp53*; *sgPten*; *sgPik3r1*; *Myc*; *Kras(G12D)* mouse endometrial cancer cells were injected into the left uterus of 8-week-old nude mice. After needle withdrawal, the incision of the enterocoelia was closed. Mice were monitored for tumorigenesis by bioluminescence imaging. Drug treatment was initiated on 14 days after orthotopic transplantation. According to the fluorescence signal intensity, mice were divided into three treatment pairs. Mice were daily treated with either vehicle or 40 mg/kg MI136 by intraperitoneal injection. Mice were analyzed by bioluminescence imaging at indicated time point. Mice were sacrificed upon the moribund.

### Bioluminescence imaging

Mice were given 150 mg/kg D-luciferin potassium salt (RegisTechnologies) intraperitoneally and imaged on a Xenogen IVIS Spectrum instrument (PerkinElmer).

## qRT-PCR

Total RNA was extracted with TRIzol (Applied Biosystems) following manufacturer's instructions. M-MLV Reverse Transcriptase was used for reverse transcription according to the manufacturer's protocol (Invitrogen). Quantitative real-time quantitative PCR (qRT-PCR) was performed using Powerup™ SYBR Green Master Mix (Applied Biosystems) in an LC480 thermocycler (Roche). The relative expression of genes were calculated using the  $2^{-\Delta\Delta ct}$  method. Gene expression was normalized to that of  $\beta$ -actin. qRT-PCR was performed on each sample in triplicate. Data was presented as relative expression of three biological replicates. The genes were selected from downregulated genes in the mRNA-seq data comparing the MI-136 group to the vehicle group. Primer sequences used to amplify mouse *Cav1*, *Nos2*, *Nos3*, *Pfkfb3*, *Serpine1*, *Cdkn1b*, *Cxcr4*, *Ep300*, *Akap12* were listed in Supplemental Table 1.

## Organoids gene editing

*Men1*, *Ash2l*, *Kmt2a*, *Hif1a* and *Hif1b*-specific sgRNA oligos were cloned into the lentiviral vector V2TC, which expresses sgRNAs and mCherry. sgRNAs were designed by the CRISPR Design Tool (<http://crispr.mit.edu/>). The lentivirus was harvested in 293T. After dissociating the organoids with TrypLE, cells were mixed with lentivirus and centrifuged for 1 hr at 2,000 r.p.m, and then incubated for 2 h at 37 °C in a culture incubator to allow transduction. The cells were then collected, spun at 1500 r.p.m. for 5 min, and replated in Matrigel as normal.

## EdU staining and confocal microscopy

EdU staining was performed with Cell-light EdU Apollo643 in vitro kit(RIBOBIO) following manufacturer's instructions. After that, organoids were incubated for 10 min at room temperature in PBS with DAPI (Sigma, D9542). Organoids were washed in PBS for 5 min three times, imaged using the Carl Zeiss Microscopy GmbH LSM880.

## RNA-sequencing analysis

RNA was extracted from organoids with the RNeasy Mini Kit (74104, Qiagen) following the manufacturer's instructions. There were two replicates in each group. RNA quality was analysed using Agilent picochips. Samples with RNA integrity number (RIN)  $\geq 7.5$  could be subjected to RNA-seq. RNA libraries were prepared for sequencing using standard Illumina protocols. The mouse RNA-seq data were sequenced with Illumina NovaSeq 6000 sequencing machine with 150-bp paired-end reads. The quality control of the RNA-seq data were carried out by Manufacturer. Raw data were firstly

processed through in-house perl scripts to obtain clean data by removing reads containing adapter, ploy-N and with low quality, and Q20(>90), Q30(>85) and GC content of the clean data meet the standard, and the clean data were used to downstream analysis. STAR was used to align the mouse RNA-seq reads to the reference genome (GRcm38) [46]. Transcript was normalized by Transcript per million(TPM). Genes with absolutely fold changes >1.3 were identified as differently expressed genes. Heatmap of differently expressed genes constructed and were normalized by z-scores. Differently expressed genes in pathway enrichment analysis and pathway network analysis were performed by ClusterProfiler [47]. GSEA used statistical approaches to identify significantly similarities and differences between two given clusters by identifying a priori-defined gene sets [48].

The intersection of downregulated genes and HIF signaling pathway genes was analyzed by VennDiagram [49], and we used HOMER to find motifs of the non-overlapping genes [50].

The RNA-seq data of human endometrial cancer and normal endometrial tissues were downloaded from TCGA-UCEC, and transcripts were normalized by DESeq2 [51]. We used ggpubr to portray the box plot of gene expression in human endometrial cancer and normal endometrial tissues. *P* values were calculated using *t*-test. Ggplot2 [52] was used to determine the correlation between *MEN1* and *HIF1A* mRNA expression in endometrial cancer tissues.

## ChIP-seq data collection and visualization

Raw data(fastq file) were downloaded from the NCBI GEO database under accession codes GSE132827, GSE85317 used Aspera. STAR was used to align the reads to the reference genome (GRch38) and peak callings were performed using MACS2. Data were visualized by Integrative Genomics Viewer (IGV) [53].

**Acknowledgements** We thank all Chen-Liu laboratory members for their invaluable discussions and technical support.

**Funding** This work was supported by the National Key R&D Program of China (2017YFA0505600).

**Author contributions** JC, LZ, YL, CC, and FN conceived the project, designed experiments, and wrote the paper. JC, HP, SD, MW, JW, YQ, ZB, YZ, and SZ performed experiments and analyzed data. LZ and JC performed RNA-seq and ChIP-seq analysis.

## Compliance with ethical standards

**Conflict of interest** The authors declare that they have no conflict of interest.

**Ethical approval and consent to participate** All the collection of specimens and animal handling in this work was reviewed and approved by the Medical Ethics Committee of the Sichuan University.

**Publisher's note** Springer Nature remains neutral with regard to jurisdictional claims in published maps and institutional affiliations.

## References

- Roy A, Matzuk MM. Reproductive tract function and dysfunction in women. *Nat Rev Endocrinol*. 2011;7:517–25.
- Jemal A, Bray F, Cente MM, Ferlay JJ, Forman D. Global cancer statistics. *CA Cancer J Clin*. 2011;61:69–90.
- Morice P, Leary A, Creutzberg C, Abu-Rustum N, Darai E, Morice P, et al. Endometrial cancer. *Lancet* 2016;387:1094–108.
- Grywalska E, Sobstyl M, Putowski L, Rolinski J. Current possibilities of gynecologic cancer treatment with the use of immune checkpoint inhibitors. *Int J Mol Sci*. 2019;20:4705.
- Lheureux S, Oza AM. Endometrial cancer-targeted therapies myth or reality? Review of current targeted treatments. *Eur J Cancer* 2016;59:99–108.
- Cherniack AD, Shen H, Walter V, Stewart C, Murray BA, Bowlby R, et al. Integrated molecular characterization of uterine carcinosarcoma. *Cancer Cell* 2017;31:411–23.
- Getz G, Gabriel SB, Cibulskis K, Lander E, Sivachenko A, Sougnez C, et al. Integrated genomic characterization of endometrial carcinoma. *Nature* 2013;497:67–73.
- Kuhn E, Wu RC, Guan B, Wu G, Zhang JH, Wang Y. Identification of molecular pathway aberrations in uterine serous carcinoma by genome-wide analyses. *J Natl Cancer Inst*. 2012;104:1503–13.
- Cheung LWT, Hennessy BT, Li J, Yu S, Myers AP, Djordjevic B, et al. High frequency of PIK3R1 and PIK3R2 mutations in endometrial cancer elucidates a novel mechanism for regulation of PTEN protein stability. *Cancer Disco*. 2011;1:170–85.
- Levine RL, Cargile CB, Blazes MS, van Rees B, Kurman RJ, Ellenson LH. PTEN mutations and microsatellite instability in complex atypical hyperplasia, a precursor lesion to uterine endometrioid carcinoma. *Cancer Res*. 1998;58:3254–8.
- Petrella BL, Brinckerhoff CE. PTEN suppression of YY1 induces HIF-2 activity in von-Hippel-Lindau-null renal-cell carcinoma. *Cancer Biol Ther*. 2009;8:1389–401.
- Bartosch C, Lopes JM, Jerónimo C. Epigenetics in endometrial carcinogenesis - part 1: DNA methylation. *Epigenomics* 2017;9:737–55.
- Salvesen HB, Macdonald N, Ryan A, Jacobs II, Lynch ED, Akslen LA, et al. PTEN methylation is associated with advanced stage and microsatellite instability in endometrial carcinoma. *Int J Cancer* 2001;91:22–6.
- Dewdney SB, Rimel B, Thaker H, Thompson DM, Schmidt A, Huettner, et al. Aberrant methylation of the X-linked ribosomal S6 kinase RPS6KA6 (RSK4) in endometrial cancers. *Clin Cancer Res*. 2011;17:2120–9.
- Seeber LMS, Zweemer R, Marchionni L, Massuger LFAG, Smit VTHBM, Van Baal WM, et al. Methylation profiles of endometrioid and serous endometrial cancers. *Endocr Relat Cancer* 2010;17:663–73.
- Suehiro Y, Okada T, Okada T, Anno K, Okayama N, Ueno K, et al. Aneuploidy predicts outcome in patients with endometrial carcinoma and is related to lack of CDH13 hypermethylation. *Clin Cancer Res*. 2008;14:3354–61.
- Guida M, Sanguedolce F, Bufo, Sardo ADS, Pannone G. Aberrant DNA hypermethylation of hMLH1 and CDKN2A/p16 genes in benign, premalignant and malignant endometrial lesions. *Eur J Gynaecol Oncol*. 2009;30:267–70.
- Daniela F, Ileana C, Barbara M, Roberta C, Emanuele D, Carlo C, et al. The high frequency of de novo promoter methylation in synchronous primary endometrial and ovarian carcinomas. *Clin Cancer Res*. 2006;12:3329–36.
- Xu S, Ren J, Bin Chen H, Wang Y, Liu Q, Zhang R, et al. Cytostatic and apoptotic effects of DNMT and HDAC inhibitors in endometrial cancer cells. *Curr Pharm Des*. 2014;20:1881–7.
- Satoshi I, Jyoji I, Keiko S. Protein expression, mRNA expression and gene amplification of DNA methyltransferase 1 in endometrial tumor tissues. *Mol Clin Oncol*. 2013;1:423–9.
- Claudia AK, Anne JV, Irmgard CL, Ulrike von R, Henning MB, Joachim A. Class I histone deacetylase expression in the human cyclic endometrium and endometrial adenocarcinomas. *Hum Reprod*. 2007;22:2956–66.
- Wilko W, Carsten D, Aurelia N, Silvia DE, Manfred D, Steve EK, et al. Expression of class I histone deacetylases indicates poor prognosis in endometrioid subtypes of ovarian and endometrial carcinomas. *Neoplasia* 2008;10:1021–7.
- Asaka R, Miyamoto T, Yamada Y, Ando H, Mvunta DH, Kobara H, et al. Sirtuin 1 promotes the growth and cisplatin resistance of endometrial carcinoma cells: a novel therapeutic target. *Lab Invest*. 2015;95:1363–73.
- Theisen ER, Gajiwala S, Bearss J, Sorna V, Sharma S, Janat-Amsbury M. Reversible inhibition of lysine specific demethylase 1 is a novel anti-tumor strategy for poorly differentiated endometrial carcinoma. *BMC Cancer* 2014;14:752.
- Bartosch C, Lopes JM, Jerónimo C. Epigenetics in endometrial carcinogenesis - part 2: histone modifications, chromatin remodeling and noncoding RNAs. *Epigenomics* 2017;9:873–92.
- Tom VN, Moiola CP, Eva C, Daniela A. Modeling endometrial cancer: past, present, and future. *Int J Mol Sci*. 2018;19:2348.
- Fatehullah A, Si Hui T, Barker N. Organoids as an in vitro model of human development and disease. *Nat Cell Biol*. 2016;18:246–54.
- Huang L, Holtzinger A, Jagan I, Nostro C, Wang RN, Muthuswamy L, et al. Ductal pancreatic cancer modeling and drug screening using human pluripotent stem cell- and patient-derived tumor organoids. *Nat Med*. 2015;21:1364–71.
- Drost J, Clevers H. Organoids in cancer research. *Nat Rev Cancer* 2018;18:407–18.
- Sachs N, de Ligt J, Kopper O, Gogola E, Bounova G, Weeber F, et al. A living biobank of breast cancer organoids captures disease heterogeneity. *Cell* 2018;172:373–86.
- Turco MY, Gardner L, Hughes J, Cindrova-Davies T, Gomez MJ, Farrell L, et al. Long-term, hormone-responsive organoid cultures of human endometrium in a chemically defined medium. *Nat Cell Biol*. 2017;19:568–77.
- Boretto M, Maenhoudt N, Luo XL, Hennes A, Boeckx B, Bui B, et al. Patient-derived organoids from endometrial disease capture clinical heterogeneity and are amenable to drug screening. *Nat Cell Biol*. 2019;21:1041–51.
- Takai N. Histone deacetylase inhibitors have a profound anti-growth activity in endometrial cancer cells. *Clin Cancer Res*. 2004;10:1141–9.
- Kiyoko U, Umene K, Yanokura M, Banno K, Irie H, Adachi M, et al. Aurora kinase A has a significant role as a therapeutic target and clinical biomarker in endometrial cancer. *Int J Oncol*. 2015;46:1498–506.
- Bestvina CM, Fleming GF. Chemotherapy for endometrial cancer in adjuvant and advanced disease settings. *Oncologist* 2016;21:1250–9.
- Shi A, Murai MJ, He S, Lund G, Hartley T, Purohit T, et al. Structural insights into inhibition of the bivalent menin-MLL interaction by small molecules in leukemia. *Blood* 2012;120:4461–9.
- Grembecka J, He S, Shi A, Purohit T, Muntean AG, Sorenson RJ, et al. Menin-MLL inhibitors reverse oncogenic activity of MLL fusion proteins in leukemia. *Nat Chem Biol*. 2012;8:277–84.

38. Malik R, Khan AP, Asangani IA, Cielik M, Chinnaiyan AM. Targeting the MLL complex in castration-resistant prostate cancer. *Nat Med*. 2015;21:344–52.
39. Salimian Rizi B, Caneba C, Nowicka A, Nabiyar AW, Liu X, Chen K, et al. Nitric oxide mediates metabolic coupling of omentum-derived adipose stroma to ovarian and endometrial cancer cells. *Cancer Res*. 2015;75:456–71.
40. Basudhar D, Glynn SA, Greer M, Somasundaram V, No JH, Scheiblin DA, et al. Coexpression of NOS2 and COX2 accelerates tumor growth and reduces survival in estrogen receptor-negative breast cancer. *Proc Natl Acad Sci USA*. 2017;114:13030–5.
41. Shi L, Pan H, Liu Z, Xie J, Han W. Roles of PFKFB3 in cancer. *Signal Transduct Target Ther*. 2017;2:17044.
42. Gustafsson NMS, Färnegårdh K, Bonagas N, Ninou AH, Groth P, Wiita E, et al. Targeting PFKFB3 radiosensitizes cancer cells and suppresses homologous recombination. *Nat Commun*. 2018;9:3872.
43. Nwosu ZC, Ebert MP, Dooley S, Meyer C. Caveolin-1 in the regulation of cell metabolism: a cancer perspective. *Mol Cancer* 2016;15:71.
44. Krivtsov AV, Evans K, Gadrey JY, Eschle BK, Hatton C, Uckelmann HJ, et al. A menin-MLL inhibitor induces specific chromatin changes and eradicates disease in models of MLL-rearranged leukemia. *Cancer Cell* 2019;36:660–73.
45. Ning Z, Jia NF, Ting CC. Synergistic combination of microtubule targeting anticancer fludelson with cytoprotective panaxytriol derived from panax ginseng against MX-1 cells in vitro: experimental design and data analysis using the combination index method. *Am J Cancer Res*. 2016;6:97–104.
46. Alexander D, Carrie AD, Felix S, Jorg D, Chris Z, Sonali J, et al. STAR: ultrafast universal RNA-seq aligner. *Bioinformatics* 2013;29:15–21.
47. Guang CY, Li GW, Yan YH, Qing YH. clusterProfiler: an R package for comparing biological themes among gene clusters. *OMICS* 2012;16:284–7.
48. Aravind S, Pablo T, Vamsi KM, Sayan M, Benjamin LE, Michael AG, et al. Gene set enrichment analysis: a knowledge-based approach for interpreting genome-wide expression profiles. *Proc Natl Acad Sci USA*. 2005;102:15545–50.
49. Hanbo C, Paul CB. VennDiagram: a package for the generation of highly-customizable Venn and Euler diagrams in R. *BMC Bioinforma* 2011;12:35.
50. Heinz S, Benner C, Spann N, Bertolino E, Lin YC, Laslo P, et al. Simple combinations of lineage-determining transcription factors prime cis-regulatory elements required for macrophage and B cell identities. *Mol Cell* 2010;38:576–89.
51. Love MI, Huber W, Anders S. Moderated estimation of fold change and dispersion for RNA-seq data with DESeq2. *Genome Biol*. 2014;15:550.
52. H Wickham. ggplot2: Elegant Graphics for Data Analysis. 2nd edn. (Springer Nature, New York, 2016).
53. Robinson JT, Thorvaldsdóttir H, Winckler W, Guttman M, Lander ES, Getz G, et al. Integrative genomics viewer. *Nat Biotechnol*. 2011;29:24–6.